

# Evaluation of optimised groyne designs in response to long-period ship wave loads at Juelssand in the Lower Elbe Estuary

Gregor Melling<sup>1</sup>, Hanne Jansch<sup>2</sup>, Bernhard Kondziella<sup>2</sup>, Klemens Uliczka<sup>2</sup> and Bettina Gätje<sup>3</sup>

<sup>1</sup> Federal Waterways Engineering and Research Institute (BAW), [gregor.melling@baw.de](mailto:gregor.melling@baw.de)

<sup>2</sup> Federal Waterways Engineering and Research Institute (BAW)

<sup>3</sup> Federal Waterways and Shipping Administration Hamburg (WSA)

## Summary

In the past 15 years, increased severity of damages to rock structures such as groynes, training walls and revetments have been observed across the major German estuaries. Investigations into the cause of the damages concluded that structure deterioration could be attributed to long-period primary ship wave loading. Owing to changes in the shipping fleet, in particular the ever-increasing dimensions of container vessels, the intensity of ship-induced loads has increased significantly. As a result, existing rock structures are, in certain parts, under-dimensioned for the presently prevalent load intensities. To evaluate the performance of two new groyne designs, optimised with a view to increase structure resistance to long-period wave loads, a prototype study was undertaken. Two groynes in the tidal Lower Elbe were rebuilt, one with a large-radius root and one with a recessed root. During the field experiment the incident ship-induced wave loading and the armour layer deformation was recorded. The field experiment and some fundamental findings with regard to the wave-structure-interaction at prototype scale and the performance of the optimised groyne designs are documented here. Furthermore, insights into mitigation measures are given, based on analyses of the collected data.

## Keywords

rock groyne, recessed groyne, ship wave, long-period wave, wave-structure interaction, overtopping, Juelssand, Elbe

## Zusammenfassung

Über die vergangenen 15 Jahre wurden in deutschen Ästuaren zunehmend Schäden an Schüttsteinbauwerken beobachtet. Als Ursache konnte die langperiodische Schiffswellenbelastung ausgemacht werden, die aufgrund der zunehmenden Schiffgröße in den letzten Jahrzehnten deutlich stärker wirkt. Als Folge sind (Ufer-)Bauwerke mancherorts für die vorherrschenden Belastungsintensitäten unterdimensioniert. Im Rahmen einer Pilotstudie wurden zwei, hinsichtlich der Stabilität der Deckschicht optimierte, Bühnenkonstruktionen untersucht. Dabei wurden zwei Bühnen in der tidebeeinflussten Unteren Elbe neu aufgebaut, eine Bühne mit ausgerundeter Wurzel und eine mit hinterströmten Bereich. Während des Feldversuchs wurden die auflaufenden schiffsbedingten Belastungen und die Entwicklung der Bühnendeckschicht aufgezeichnet. Die Durchführung des Feldversuchs sowie einige grundlegende Ergebnisse hinsichtlich der Schiffswellen-

*Struktur-Interaktion im Naturmaßstab und die Eigenschaften der optimierten Bubnenkonstruktionen werden hier dokumentiert. Des Weiteren werden, basierend auf Auswertungen der erhobenen Daten, Hinweise hinsichtlich der Möglichkeiten zur Reduzierung von Schäden an Schüttsteinbuhnen gegeben.*

## Schlagwörter

*Buhne, hinterströmte Buhne, Schiffswelle, lang-periodische Welle, Wellen-Struktur-Interaktion, Überströmen, Juelsand, Tideelbe*

## 1 Background

### 1.1 Engineering issue

In the past 15–20 years, increased severity of damages to rock structures such as groynes, training walls and revetments have been observed across the major German estuaries (e.g. Ohle and Zimmermann 2003, WSA Bhv 2009, BAW 2010, WSA HH 2010, BAW 2012). In response, using practical engineering judgement, different measures to increase the stability of training walls and groynes were undertaken. These included shallower slope angles, reduced crest widths as well as wider groyne root areas and smoother revetments transitions (WSA Bhv 2009, WSA Cux 2012). While mitigation measures were taken, the processes and mechanisms underlying these damages remained poorly understood. Investigations into the cause of the damages were subsequently carried out by BAW (2010) which confirmed that structure deterioration could in large part be attributed to long-period ship wave loading. Owing to changes in the shipping fleet, in particular the ever-increasing dimensions of container vessels, the intensity of ship-induced loads on estuary infrastructure has increased significantly. Ship-induced loads have over the recent years become the most relevant hydraulic loading in German estuaries with major shipping lanes. As a result, existing rock structures are, in parts, under-dimensioned for the presently prevalent load intensities. Looking into the future it is expected that ship-induced loading will further increase with continuing trends towards greater vessel sizes and increased traffic density. Also, the percentage of all waterway traffic associated with ultra large container vessels (ULCV) of the “New Panamax” and “Triple E” categories is likely to increase.

### 1.2 State of the research

While the described engineering problem is becoming increasingly common in German waterways, interestingly, a survey of European and international coastal/waterway engineering bodies and research institutes in 2012 resulted in the feedback that structural damage in response to long-period ship waves is not currently seen as a significant problem and is mitigated either by vessel speed restrictions or implicitly accounted for in structure design (cf. BAW 2012). Nevertheless, in recent years various impacts associated with the long-period wave, alternatively termed “Bernoulli wake”, “depression wake” or “hull displacement wave” by other authors, have become increasingly apparent in other countries (e.g. Ravens and Thomas 2008, Rapaglia et al. 2011, Gelinis et al. 2013, Göransson et al. 2014, Zaggia et al. 2017). While these studies have been primarily concerned with the impact of long-period ship waves on sediment transport, morphodynamic effects and bank erosion,

none have been focussed explicitly on the stability of with rock structures. Nevertheless, existing studies contribute to the understanding of the behaviour of long-period waves in shallow and confined waterways as well as demonstrating their erosive capacity.

Rapaglia et al. (2011) investigated the drawdown-related resuspension of sediments in Venice Lagoon and reported flow velocities greater than 2 m/s associated with the trough of the primary wave. Sediments are transported in the direction of the shipping channel, with channel maintenance implications. Similarly, in Venice Lagoon, Scarpa et al. (2019) describe the erosive effects of the depression wave in tidal flats. High rates of shoreline retreat were also associated with the action of the long-period depression wave. As very large depressions of up to 2.45 m were recorded, the authors posit that the drawdown depression wave can be amplified by shoaling and wave transformation effects in the channel margins, eventually transforming into a sharp-crested travelling solitary depression wave, with significant vertical velocity components. The height of the drawdown was linked to Froude-Number and displaced water volume. As mitigation measures, speed restrictions and the optimisation of ship hull shapes are discussed. The transformation of the depression wave in shallow areas into a bore-like feature resembling a non-linear solitary Riemann wave is also described by Parnell et al. (2015). Göransson et al. (2014) report that in Göta Älv, the measured turbidity maximum was dependent on drawdown height, but that both primary and secondary ship waves are responsible for shoreline steepening and erosion effects. Measurements in the Kiel canal revealed that while there are strong dependencies between hull geometry the primary wave and associated near-bottom return-flow velocities, the turbidity maximum was correlated most nautical parameters, but only weakly (Niehüser et al. 2016). Based on these measurements Ulm et al. (2020) concluded that approx. 10 % of the total sediment transport can be attributed to vessel traffic, indicating that morphological effects of shipping can play a relevant role in the maintenance cost of waterways. In a similar vein, Zaggia et al.'s (2017) analysis of survey and remote sensing data showed that in relatively sheltered settings such as estuaries and lagoons with heavy vessel traffic the morphological evolution can be dominated by shipping-related effects, surpassing natural erosive agents such as storms. The authors note not only the shear-stresses induced from the drawdown but also the erosive effects of the trailing primary wave on adjacent beaches and erosion scarps. Regression rates of up to 4 m/year are reportedly associated with shipping effects.

With increasing vessel dimensions and draughts as well as increasing traffic density, it is not unlikely that adverse effects from primary ship waves will become more widespread and prevalent in tidal waterways in the future, affecting the function and condition of man-made shoreline infrastructure, such as sluice gates, embankments, training walls and groynes, which are the focus of this study. With a view to developing guidance and methods for rock groyne design, BAW, in cooperation with several university partners, devised a multi-faceted research framework in which the wave-structure interaction was investigated in significant detail. The research reflects the current state-of-the-art for groyne design with respect to long-period wave loading. A detailed summary of the individual work packages and their respective findings is available in BAW (2018). Here, only a brief overview of the conducted research shall be given in order to provide the necessary context for the presented work.

The early research from BAW (2010) and BAW (2012) focused on descriptions of the observed damage patterns for different rock structures in German estuaries and a process-

based understanding of the load cases and damage mechanisms. Conceptual models of the loading and failure mechanisms were proposed and in-situ pressure measurements at Langlütjen training wall in the Outer Weser were undertaken to validate the theoretical models. A detailed assessment and description of the wave-structure interaction and damage mechanisms was conducted by Gier and Schüttrumpf (2012) and a freeboard-dependent classification of the various load cases was developed. An investigation into available design equations for the most damaging load case concluded that the stability of existing groynes could not be confirmed. Furthermore, it was concluded that guidance for structure design in response to (wind) wave loading (e.g. Hansen 1985, EAK 2002, CIRIA et al. 2007), while applicable for secondary ship waves, does not adequately account for the processes associated with long-period wave loading, in particular highly turbulent overtopping flows, and is thus not applicable. In fact, the relevant processes resemble more closely those found at rockfill dams, spillways and overtopped embankments as will be explained in more detail below.

Oumeraci and Brühl (2013) investigated field and lab measurements of ship waves in an attempt to develop an analytical model for wave generation and propagation. This included the classification of different wave types and generalised wave characteristics based on ship type, speed and channel geometry. Frequency analysis is used to determine the spectral characteristics of the long-period wave component and identify wave parameters that are relevant for structure design. Small-scale 2D flume tests were carried out with the aim of determining the overtopping volumes for stationary flow, short-period waves (Wöffler et al. 2015) and long-period waves (Oetjen et al. 2017) for model bodies with different cross-sections and porosities. For the stationary overflow load case, using the measured overflow volumes on different cross-sections, weir coefficients for the Poleni-formula were derived. For short-period wave loading, the overtopping volumes as a function of freeboard height, armour layer porosity and surf similarity parameter for different model geometries were determined. At very long wave periods the overtopping flow can temporarily resemble the previously examined (quasi-)stationary flow situation and modified weir coefficients were determined. For the long-period load case, armour layer stability in response to a single surge-like wave was investigated. An attempt was also made to replicate the stationary flow tests in a numerical model with the aim of carrying out armour layer stability assessments by means of coupling a detailed flow model (CFD) with a model of structural dynamics of the rock armour layer (CSD); the efforts are documented in Oumeraci et al. (2014).

Based on an understanding of the structural response to the most relevant load cases and taking cues from the characteristic patterns of damage observed in the field as well as existing experiences with profile optimisation (WSA Bhv 2009, WSA Cux 2012) groyne designs with an expected greater structural stability to long-period wave loading were developed. Compared to the conventional groyne design, the modifications resulted in shallower slope angles on the sides and head area as well as two different configurations of the root area, i.e. where the groyne attaches to the existing revetment. The hydraulic performance of these innovative geometries was evaluated in 3D physical model tests in a wave basin by BAW (2015) at 1:40 scale. Apart from the measurement of waves and currents in the near-field of the structures and the groyne fields, the depth of the overtopping flow on the groyne crest was recorded. No investigations of armour layer stability were conducted.

The research programme culminated in a prototype-scale field study of two groyne designs, facilitated by close cooperation with the Federal Waterways and Shipping Office Hamburg (WSA). Following the findings of the aforementioned physical model tests, one groyne with a large-radius root and one with a recessed root were built. To record the incident wave loading and document the structural response an elaborate monitoring programme was implemented which has resulted in a unique dataset of load and resistance information. This dataset allows for detailed examination of the wave-structure-interaction at prototype scale and can also be used in the development of design guidance for the sizing of rock armour layers on groynes. The aim of this paper is to document the set-up and execution of this field experiment as well as some primary results and findings.

## 2 Wave-structure-interaction

### 2.1 Long-period primary ship waves

For large vessels in relatively narrow waterways, the long-period ship wave can present the most relevant load with respect to shoreline infrastructure stability. Figure 1 illustrates the primary and secondary wave systems associated with a ship travelling in confined and shallow water. The primary wave system consists of a bow wave followed by a water level depression caused by a pressure drop around the vessel hull, and a transverse stern wave. This long-period wave system is hydraulically bound to the ship hull and thus travels along the shoreline at a rate equal to the vessel speed. Following the passing of the stern wave, the water level drawdown is compensated with the slope supply flow which works to restore the ambient water level. The period  $T_{Hp}$  of the primary wave is determined by vessel length and its speed over ground (SOG); for the current vessel fleet structure in the Elbe Estuary values of approx.  $60 \text{ s} < T_{Hp} < 120 \text{ s}$  are typical.

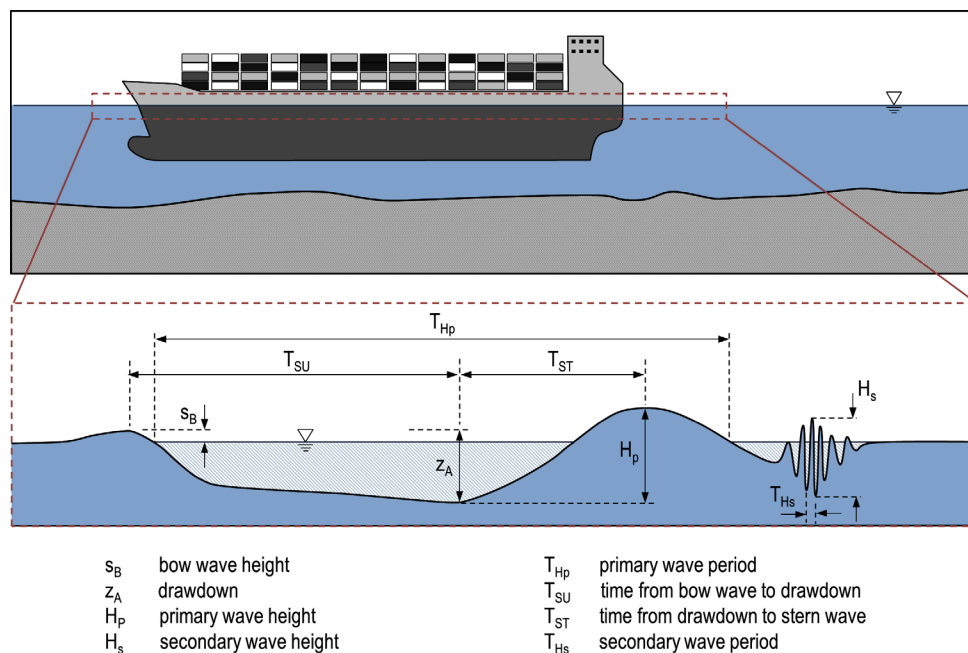


Figure 1: Schematic illustration of the ship-generated wave system in confined shallow water with idealised ship wave record and definition of characteristic parameters.

The interaction of a primary wave ( $T_{Hp} = 95$  s) with a groyne at approximately mean water level (freeboard  $R_c \approx 0$ ) is illustrated by a series of time-lapse photographs in Figure 2. The interaction begins with the bow wave (Figure 2a), typically small with negligible impact (here  $s_B = 0.1$  m), followed by the drawdown ( $\zeta_A = 0.7$  m) which causes a water level drop in the upstream groyne field. The resulting water level gradient results in compensatory flow over the groyne opposite to the direction of travel (Figure 2b, c). This flow situation weakens as the vessel, and the drawdown, gradually moves into the downstream groyne field and the original water level in the upstream groyne field begins to be restored (Figure 2d). This is associated with the arrival of the transverse stern wave and the water-level-restoring slope supply flow. The drawdown in the downstream groyne field now acts to reverse the water level gradient and results in a flow over the groyne in the direction of travel (Figure 2e).

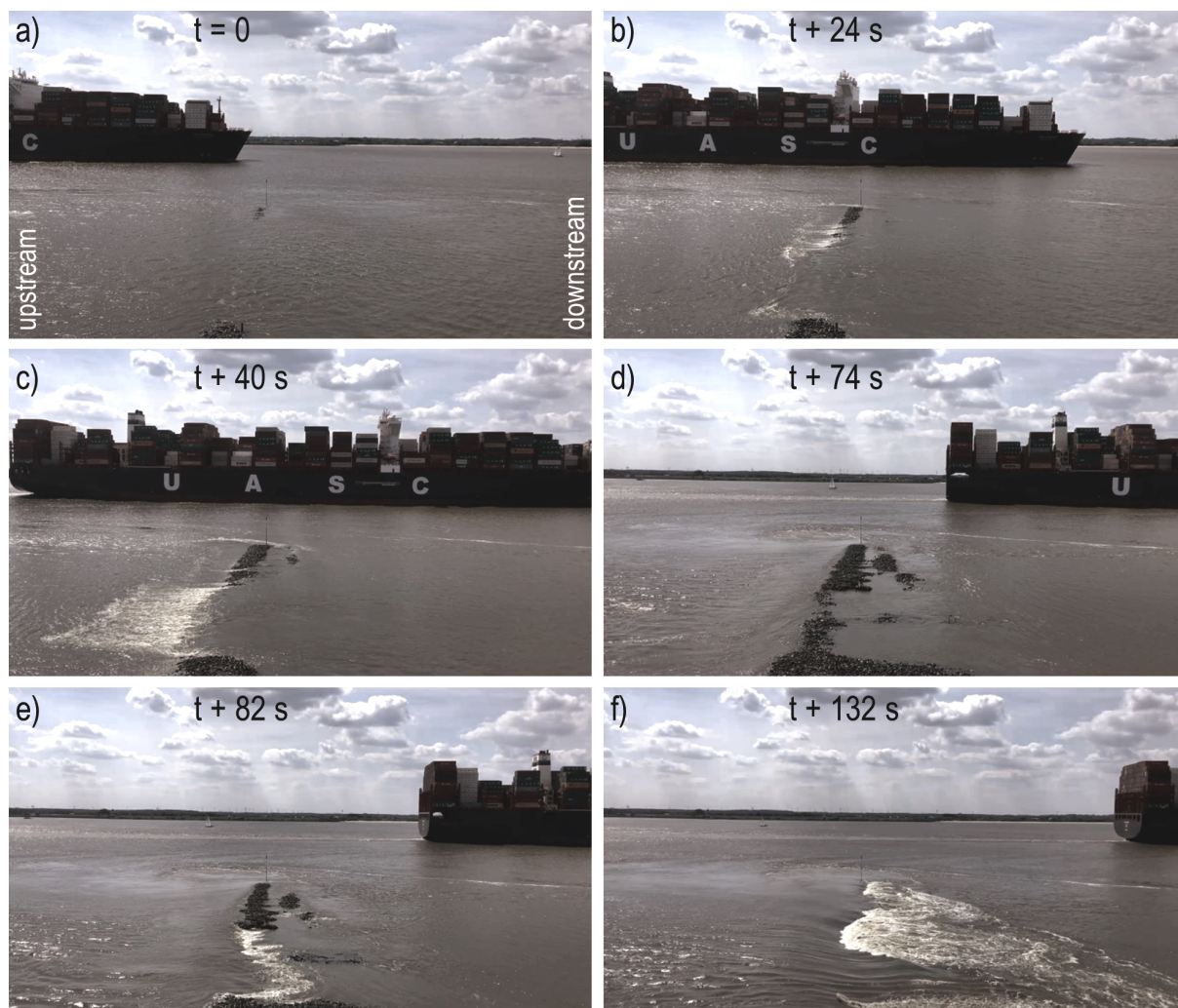


Figure 2: Interaction of long-period ship wave with groyne at Juellssand (Lower Elbe Estuary) during passage of seaward-travelling ULCV (length 368 m, breadth 51 m) at approx. mean water level. Passage with draught of 12.5 m, 13 kn  $STW$  and passing distance  $d$  of 228 m.

Due to wave focussing effects, which lead to a concentration of energy in the root area, the overflow typically initiates here and subsequently spreads along the groyne towards the head. The large gradient and the surge-like action of the transverse stern wave ( $H_p = 0.71$  m) results in a relatively shallow-depth (depending on tidal water level) overflow

that is characterised by high velocities and strong turbulence; flow aeration on the lee side is also common, the extent varies with the hydraulic configuration of the overflow and boundary effects (Figure 2f). The described processes are representative of the load case for freeboards in the approximate range  $R_c \lesssim 0$ . For positive freeboard heights overflow phenomena may be weaker, restricted to lower parts of the groyne or replaced by stronger flows around the head of the groyne; in this case wave run-up, wave breaking and overtopping processes are dominant.

## 2.2 Structure response

The structural response of groynes under long-period ship wave action is described in detail in BAW (2010) and BAW (2012). At the study site, the groynes exhibit a characteristic pattern of damage that features the deterioration of the groyne root to the point of complete destruction and deformation of the crest, particularly on the lee side, w.r.t. the incident wave (cf. Figure 3).



Figure 3: Characteristic damage to groynes at Juelssand (Lower Elbe Estuary) caused by long-period ship wave action. Destruction of the groyne root (left) and erosion of the crest and lee side slope (right).

Different load cases are relevant depending on water level and freeboard height. A differentiation of the load cases  $R_c > 0$  and  $R_c \lesssim 0$  is useful, as the processes and damage mechanisms are distinct and typically also affect different areas of the groyne, as illustrated conceptually in Figure 4.

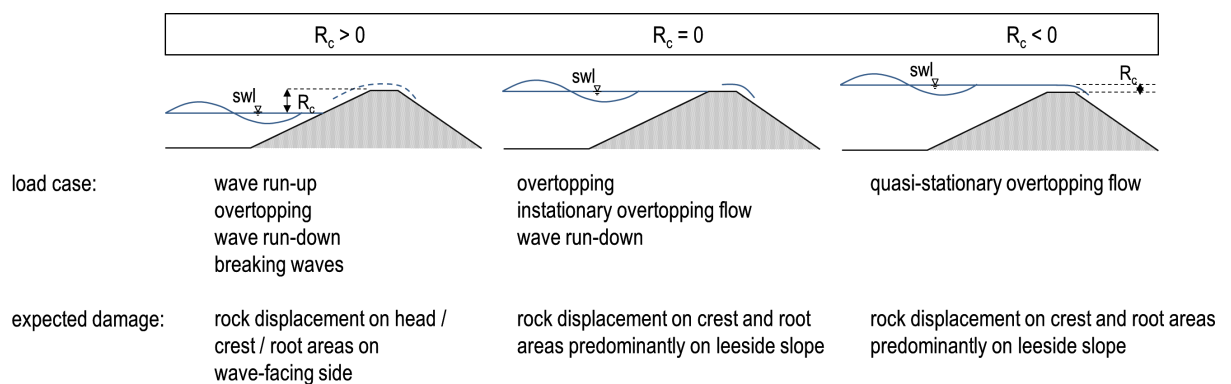


Figure 4: Conceptual model of load cases and associated damage due to long-period primary ship waves in relation to freeboard  $R_c$ . Modified from Gier and Schüttrumpf (2012).

For positive  $R_r$ , wave impact processes are prevalent, affecting mostly the wave-facing slope (in this publication “wave-facing” is used with respect to stern waves from outgoing ships), although some overtopping and wave run-down on the lee side is possible, depending on structure parameters such as crest height and permeability. For  $R_r \lesssim 0$  the forces on the armour layer are related primarily to overflowing of the groyne. In this case, the structural response to supercritical loading is expected in the lee portion of the root and crest areas. Gier and Schüttrumpf (2012) conclude that the long-period wave is particularly damaging due to the fast-flowing and highly-turbulent overflow of the groyne.

### 3 Prototype field study

#### 3.1 Site description and loading factors

Juelssand is located on the northern bank of the Lower Elbe Estuary, along the main access channel to the Port of Hamburg, between chainage km 651–653 (Figure 5). The groynes here are already experiencing significant structural deterioration from ship waves (cf. Figure 3); the site is thus an ideal site for the pilot study. For this purpose, groynes B29 and B31 were rebuilt using optimised designs. Mutual interferences stemming from changes to the loading regime as a result of the rebuilding of the groynes are eliminated by keeping the intermediary groyne B30 in its current state.

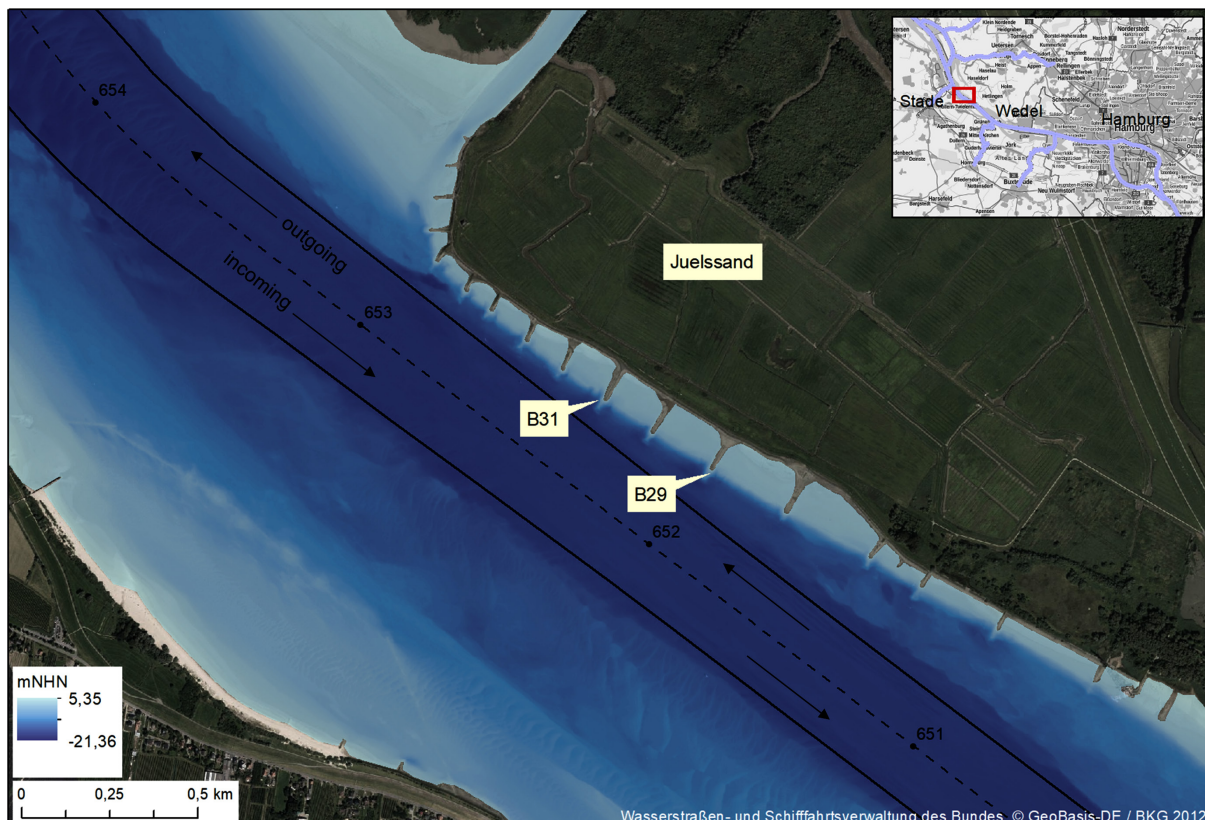


Figure 5: Location of study site at Juelssand with pilot study groynes, indicative bathymetry, location of navigational channel and chainage.

### 3.1.1 Fairway characteristics

Owing to the proximity of the shipping channel to the shoreline, this area is characterized by close passing distances and significant ship wave energy, especially in the case of seaward travelling vessels. The distance from groyne tip to the edge of the fairway can be as short as 65 m. The channel side is very steep with slopes of approx. 1:5 (cf. Figure 5).

### 3.1.2 Vessel fleet structure

Based on an examination of Automatic Identification System (AIS) data, the distribution of vessel sizes for which wave events were registered during the monitoring period is shown in Figure 6. The vessel sizes are relatively evenly distributed, although vessels of the New Panamax type (on average 366 m length, 49 m breadth) constitute the dominant ship in terms of loading frequency with over 12.5 % of recorded wave events attributable to this class. Approximately 4 % of recorded wave heights originated from the currently largest ULCVs (length > 395 m, breadth > 53 m) sailing on the Elbe Estuary.

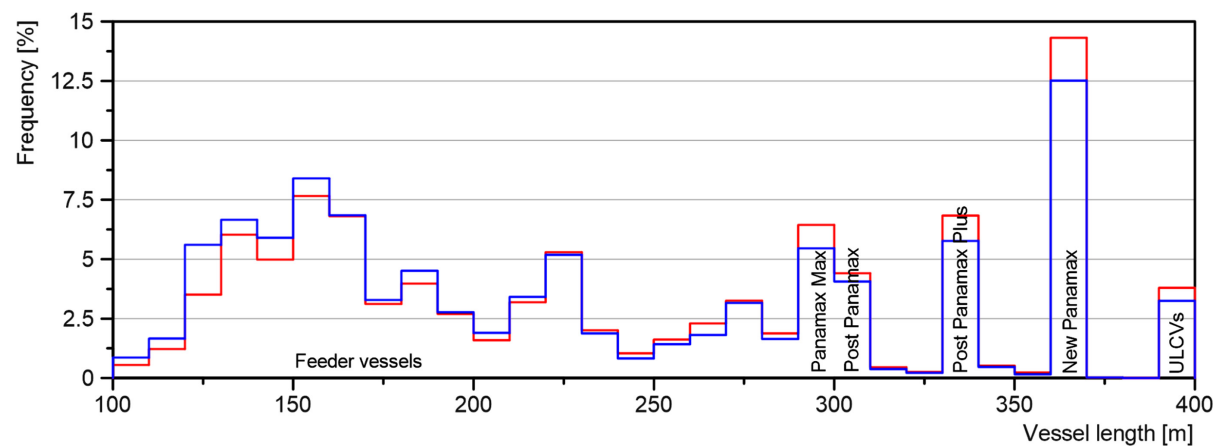


Figure 6: Distribution of vessel length for wave events registered at position 1 at B29 (red) and B31 (blue).

### 3.1.3 Speed restriction

In January 2018, a speed restriction of 12 kn *STW* for vessels with lengths greater 90 m was instated in this part of the Elbe Estuary. In response, the statistical distribution of ship speeds has changed significantly as shown in Figure 7. The median speed shows a reduction from 13.8 and 13.5 for B29 and B31, respectively to 12.5 kn. Crucially, the occurrence of large velocities above 15 kn is significantly reduced.

The speed restriction falls within the monitoring period and must be taken into account when interpreting rock armour stability. Since AIS data only provides the speed over ground (*SOG*), current velocity data from an operational model (see Section 3.3.3) was used to derive the corresponding *STW* for each vessel.

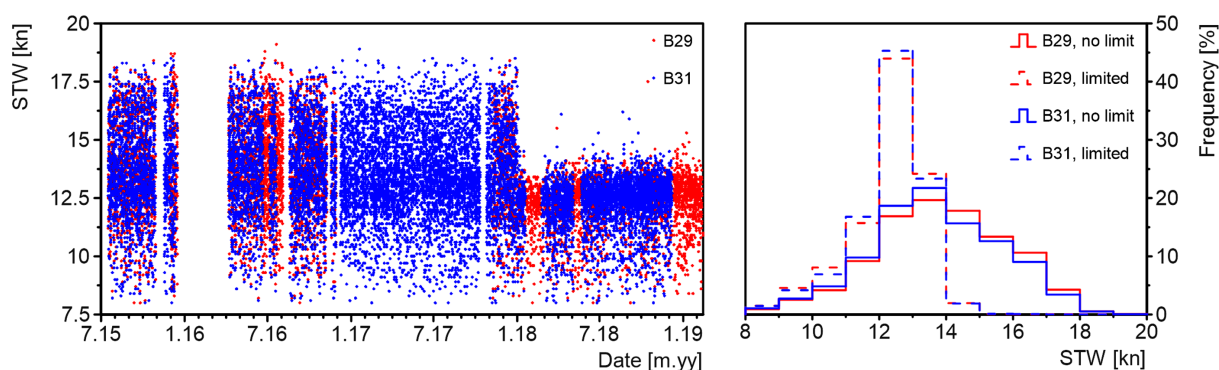


Figure 7: Change of  $STW$  with time (left) and distribution of speeds before and after introduction of speed limit (right).

## 3.2 Groyne designs

### 3.2.1 Conventional design

The conventional design follows a two-layered approach. However, the core material is often pre-determined by the remnants of historical groyne construction. The armour layer in this area consists of CP<sub>90/250</sub> rock grading, typically with high-density iron-silicate rock with a specific density of approx. 3.4t/m<sup>3</sup>. The cross-sectional geometry is characterised by a crest width of 2.0 m and side and head slopes of 1:3 and 1:4, respectively.

### 3.2.2 Optimised groyne designs

For the new groyne types, shallower slope angles were used, as well as a higher crest level (Figure 8). The crest width was reduced and rounded to produce a “chevron”-shaped crest. The difference between B29 and B31 is related to the configuration of the groyne root and revetment transition. The characteristic pattern of damage (cf. Figure 3) and the understanding of wave-structure-interaction point to the fact that the most vulnerable part of the groyne is the root area due to the focussing of wave energy. Hence, two design solutions were implemented in this area with the aim of increasing rock armour stability by reducing loading in vulnerable areas of the groynes. At B29 the transition area from groyne body to revetment was fashioned as a 25 m wide recess (at its narrowest point) with scour protection (Figure 8, Figure 9). The intention is to allow wave energy to bypass the structure thus minimising focussing effects in the root area which lead to overtopping flows on the groyne body. At B31, the transition to the revetment was profiled to a larger diameter radius of 25 m with the intention of reducing wave focusing and strengthening the groyne in the root area.

Initially, both groynes were reconstructed using the original rock grading of CP<sub>90/250</sub> in order to assess the efficiency of the geometrical optimisations for increased erosion resistance of the armour layer. These structure variants are referred to as B29v1 and B31v1, respectively. During the study, groyne B29 was later re-profiled using larger rock grading LMB<sub>5/40</sub> (high-density rock) and monitored for a further 1.5 years. This variant is referred to as B29v2. The existing revetment in the study area was not changed.

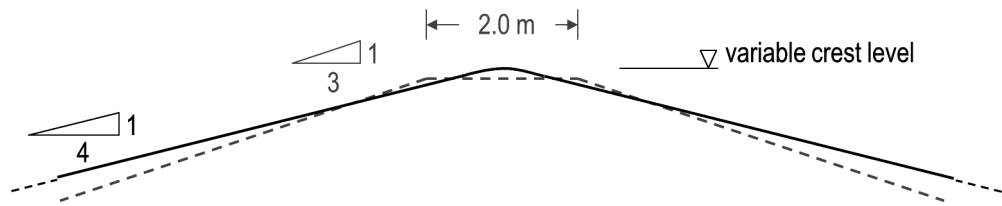
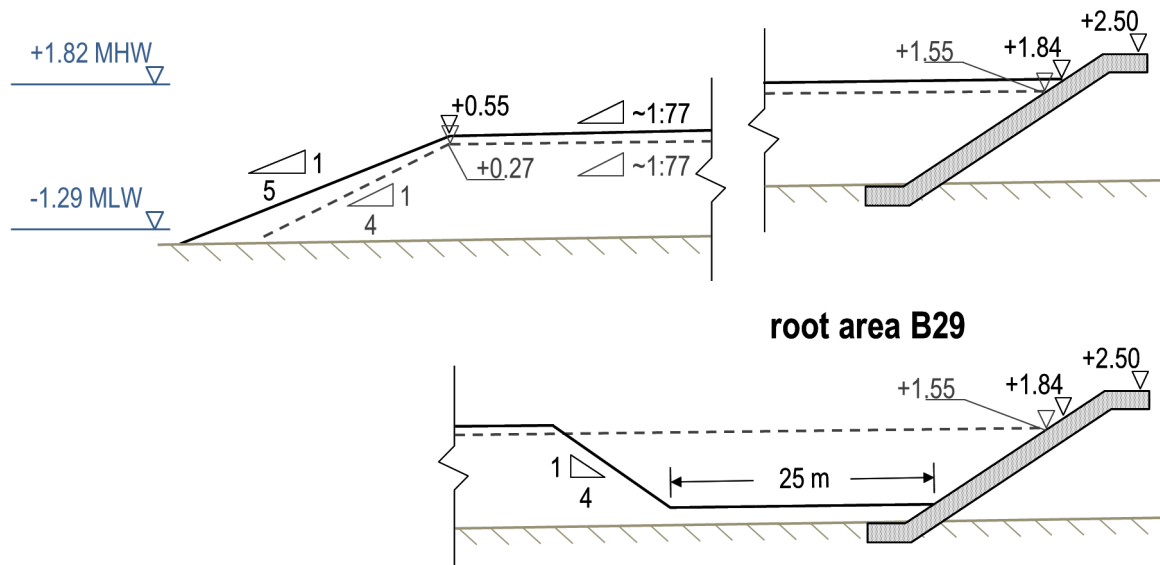
**cross section****longitudinal sections**

Figure 8: Comparison of conventional groyne profile (grey dashed) and optimised design profile in pilot study (black). All levels in mNHN. Not to scale.

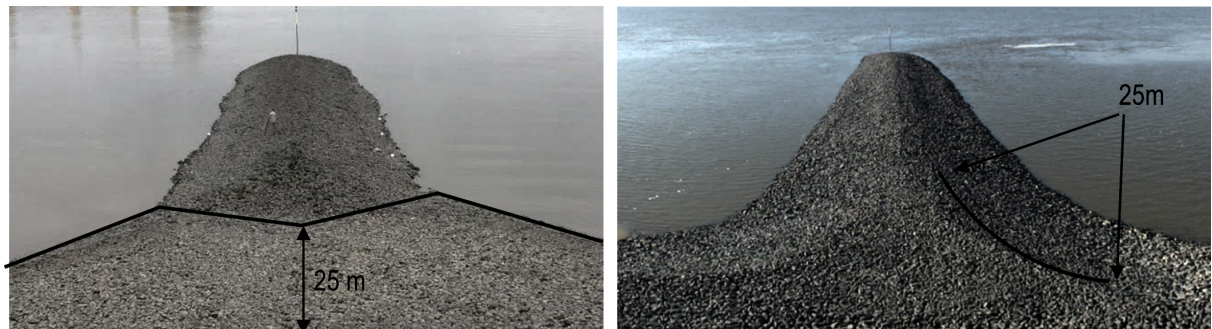


Figure 9: Photographs of the optimised groyne root designs taken from the crest of the revetment: recessed root (B29, left) and large radius root (B31, right).

**3.3 Monitoring**

The scope of the monitoring programme was defined with the intention of:

- capturing the processes relevant to the wave-structure interaction
- validating the conceptual failure models at prototype scale
- carrying out analyses of the relationships between loading, resistance variables and influencing factors such as nautical (ship and waterway) parameters
- gathering the data required for the development of design methodology

With these aims in mind, it was necessary to gather sufficiently long time-series of loading and resistance parameters. Due to the protected nature of the site as a designated nature conservation area as well as reduced accessibility of the site, it was necessary to ensure a high degree of autonomy of the measuring systems in terms of power supply, data storage, data transfer and troubleshooting. Still maintenance intervals of 2–4 weeks were required to ensure continued operation of the instruments. The necessary infrastructure for the deployment of the instruments was installed in 2014 and a trial phase was initialised in order to test and validate the systems. The official monitoring programme began in July 2015 and ran through until February 2019. The dataset generated by the monitoring programme contains over 2000 records of groyne topography recorded at low tides and between 5000–26000 ship-related wave events, depending on groyne and exact measurement location.

### 3.3.1 Structure response

To document the spatial and temporal groyne damage development, the topography of the armour layer was recorded by means of a stationary land-based 3D geodetic monitoring system developed and operated by BAW in cooperation with the HafenCity University Hamburg. The technical details of the monitoring set-up are documented in detail in Tschirschwitz et al. (2016, 2017); here, only a brief description of the most important features is given.

The geodetic monitoring system for each groyne consists of a terrestrial laser scanner (Zoller+Fröhlich IMAGER 5010) as shown in Figure 10 encased in a custom-built secure weather-proof housing and mounted on a monitoring platform at a height of 12 m above ground. The masts which elevate the monitoring platforms were installed by the WSA Hamburg and secured in position by four steel cables to reduce lateral movement and leaning due to wind and movements in the marshy subsoil. Power to the equipment is supplied by a solar panel, a small wind turbine and a fuel cell.

Terrestrial laser scanning was chosen due to the requirements for automation and sufficient areal coverage. Furthermore, a high resolution is required to detect the smallest changes in groyne topography; this allows even small movement of rocks in the armour layer to be identified and associated to loading conditions. The theoretical spatial resolution achievable with the described system at the groyne tip, determined by the angle of ray incidence and angle resolution, is given as 1 cm (Tschirschwitz et al. 2016). However, this theoretical value is significantly reduced as the result of the particular challenges of this application and operating environment. Shallow survey angles of as low as 5°, particularly towards the groyne tip, give rise to shadowing effects owing to the rough and undulating surface of the armour layer. Not limited to shallow survey angles, the strength of the optical return signal can be significantly weakened by absorption and scattering on the dark, irregular and often wet surface. This can be exacerbated by weather and meteorological effects. Measurements can have a degree of ambiguity due to artefacts, spurious measurements or real obstructions, such as seagulls sitting on the structure. As a result, measurement errors can accumulate and not all scans are viable. Nevertheless, by means of diligent post-processing the plausibility, viability and accuracy of the scans can be ensured; ambiguous scans that cannot be sufficiently corrected are removed to ensure coherence of the dataset used for further analysis.



Figure 10: Set-up for monitoring of groyne topography at low tide levels with pile-mounted laser scanners. Close-up of the monitoring platform with laser scanner housing.

The damage development is calculated in post-processing by a comparison of the measured point cloud with the reference measurement. For this purpose, the cloud-to-cloud distance function of Cloud Compare, an open-source software, is utilized. This function calculates for each point of the measured cloud a horizontal and vertical distance to the reference cloud using the nearest neighbour distance, a kind of Hausdorff distance algorithm. The vertical distance to the reference model determines the deformation of the rock armour layer. The difference plot is presented as a grid of 1 m, 0.5 m and 0.25 m resolution where the centroid values are given by the mean of the measured elevations in this raster cell. This raster is used in the interpretation of damage.

### 3.3.2 Hydraulic loading

The changes to the water surface level at the structure were measured with pressure sensors positioned at various locations in the head, foot, root and crest areas of the groynes (cf. Figure 11). Pressure sensors by Driesen & Kern and RBR were used with a sampling rate of 1 Hz. The data loggers were installed in the rock armour layer in order to measure pressure fluctuations at the structure level. For this purpose, metal tubing, in which the instruments were housed, were driven into the armour layer as illustrated in Figure 11. The data loggers were exchanged on an approximately three-weekly rotation in order to recharge the batteries and download the data before the internal data memory was exceeded. Post-processing of the raw measurements includes:

- correction for time drift of the internal clocks
- conversion of pressure to water depth, applying the barometric pressure of a nearby weather station

- filtering the data with a high-pass filter with cut-off frequency of 1/1800 Hz (30 min) in order to separate ship-induced and tidal contributions to the pressure signal
- filtering the ship-induced components with a low-pass filter at a cut-off frequency of 1/10 Hz (10 s) to derive a clear signal of the long-period ship waves
- extracting wave events and determining the relevant parameters of the long-period ship wave (cf. Figure 1)
- correlating the wave events with AIS data

The wave measurements used here encompass the time period of the experiment from 07/2015 to 12/2018 for B31 and 02/2019 for B29. Due to maintenance intervals, failures and seasonally reduced number of monitoring positions, the record length can vary strongly between individual sensor locations. Nevertheless, typically a record length of at least 10,000 wave events is available, bar at position 6, where due to the location on the crest fewer events are recorded.

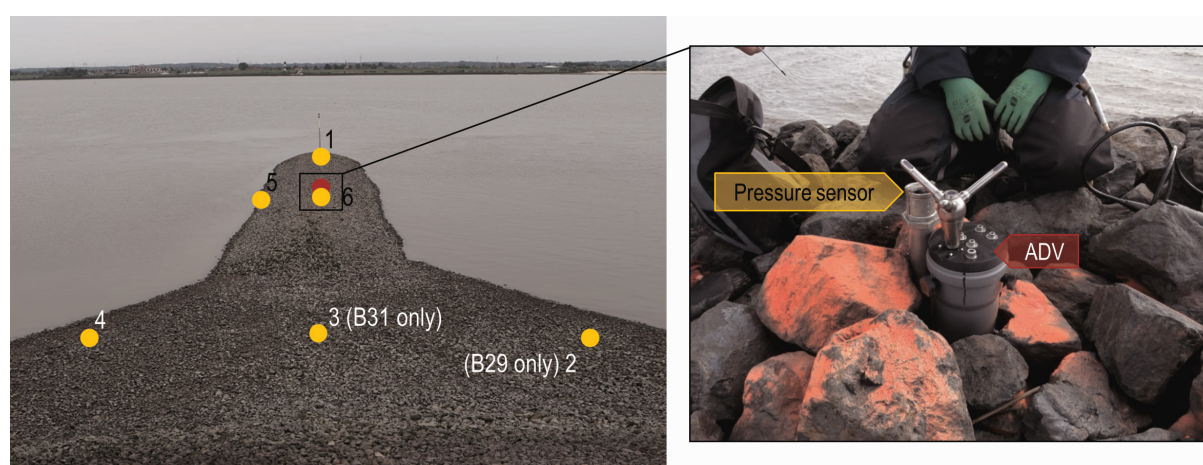


Figure 11: Distribution of pressure sensors (yellow) and current meter (red) (left). Current meter only deployed at B29. Set-up and housing of current meter and pressure sensors (right).

Coinciding with the strengthening of groyne B29v2 and recognizing the significance of overtopping loads, a Nortek Vector single-point acoustic-doppler-velocimeter (ADV) was installed on the crest to measure overflow velocities. Similarly to the pressure sensors, the instrument was encased in a plastic tube and installed in the rock armour, approximately 0.2 m above crest level (cf. Figure 11); this puts the point at which the velocities are measured at roughly 0.35 m above crest level. The orientation of the device was set to align the x-axis parallel to the expected flow. The sampling rate was 32 Hz. Post-processing consists of:

- correction for time drift of the internal clocks
- high-pass filter to separate ship induced current from tidal current
- detecting overflow events
- determining the relevant parameters of the ship-induced currents and overflow event
- correlating the wave events with AIS data

The measurement of flow velocities on the groyne crest was undertaken for approx. eleven months (net) between 11/2017–12/2018. Monitoring of primary wave loads at groyne B29 is ongoing – in a much reduced scope – with pressure measurements at positions 1 and 5 and regular visual and photographic assessments of groyne development.

### 3.3.3 Other data

Other data sources include AIS data of vessel traffic which contains information on nautical parameters (e.g. vessel dimensions, draught, speed through water and passing distance). Trimonthly profile surveys of topography in the groyne fields are also available from WSA Hamburg, allowing the influence of the designs on the adjacent beach levels to be examined. Meteorological data was sourced from a nearby weather station run by the DWD (Deutscher Wetterdienst). Where needed, current velocity data was extracted from an operational hydrodynamic model of the Elbe Estuary (PROPTTEL), as described in Sehili et al. (2014).

## 4 Analysis of prototype observations

### 4.1 Hydraulic loading

The loading regime is described by means of statistical analyses of the pressure and flow velocity measurements. For this, the available record length in the time period 07/2015 to 12/2018 (B31) or 02/2019 (B29), minus obvious errors and outliers, is typically used unless stated otherwise. As mentioned above, the sample size varies at each sensor location. For the purpose of documenting preliminary results, statistics for the entire monitoring period are given. Some caveats to the interpretation of results associated with this approach will be discussed in section 5.1.

#### 4.1.1 Long-period wave heights

The statistical distribution of wave heights at the measurement locations is shown in Figure 12. Comparing the wave heights at the groyne heads which are mostly undisturbed from the effects of wave-structure interaction a similar distribution of  $H_p$  magnitudes is observed. Over 90 % of incident primary wave heights are below 0.5 m. Differences in the wave regime at this location appear marginal, with a slightly higher median wave height at B31. The measurements at the other locations are more strongly influenced by the specific structure geometry. At B29 the maximum  $H_p$  was recorded at position 5, however, on average, larger waves are encountered further toward the root area at positions 2, 3 and 4.

In terms of large wave heights, arbitrarily defined here as  $H_p > 1.0$  m, only 5.6 % of observations satisfy this condition at position 4. At B31, the largest waves are also experienced in the root area, however the heights are greater. At position 4 over 10 % of the wave heights exceed 1.0 m and just over 3 % exceed 1.5 m. The comparison of wave heights at the groyne crests (pos. 6) suggests that somewhat higher loads are experienced at B31 and a larger number of events exceeding 1.0 m.

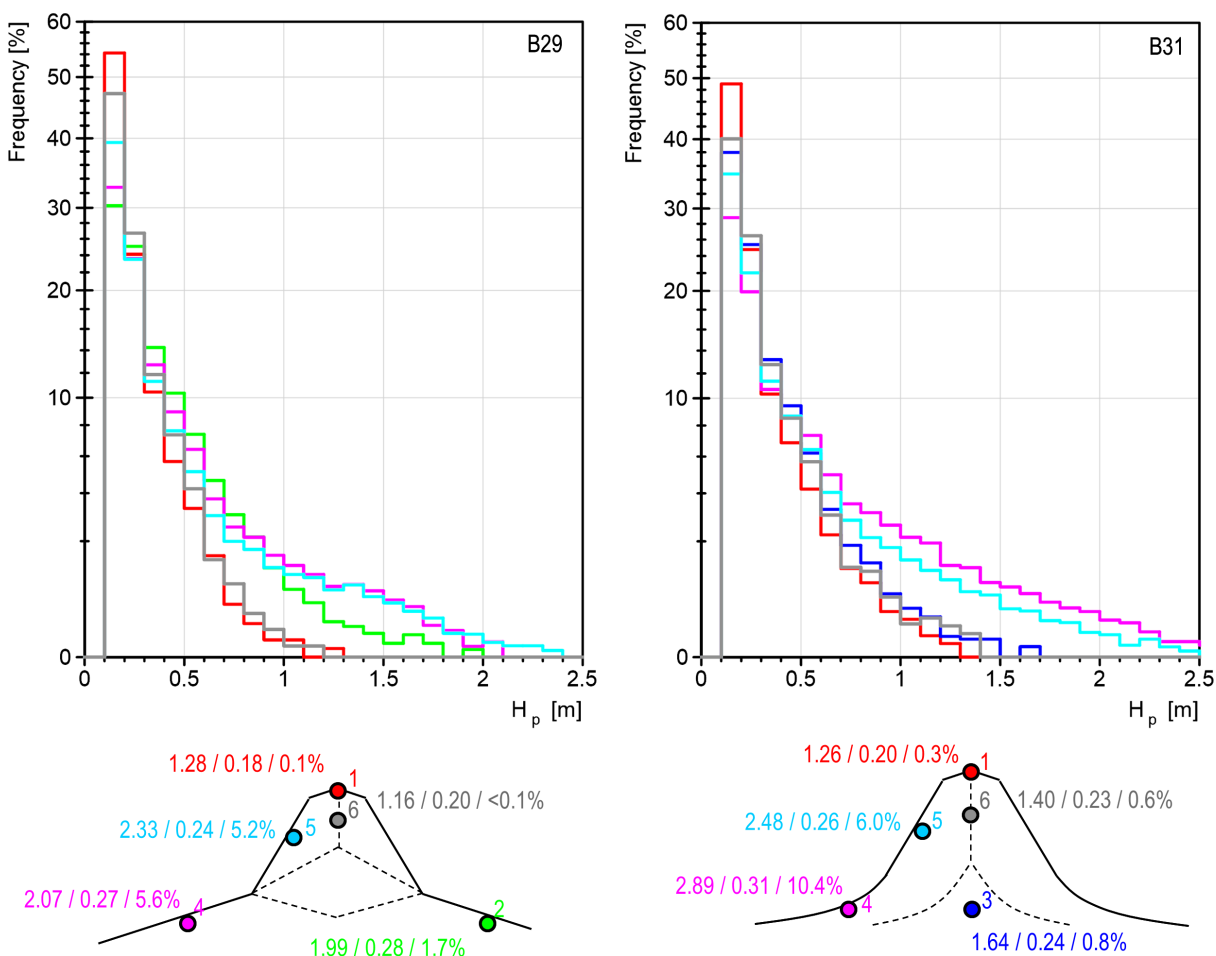


Figure 12: Histograms of wave heights at measurement locations (top).  $H_{p,max}$  /  $H_{p,med}$  / %  $H_p > 1.0$  m given for each measurement location (bottom).

### 4.1.2 Overtopping flows

The occurrence and nature of overflow phenomena over the groyne crest are a function of the water level, the incident primary ship wave height and wave-structure-interaction effects. As such, overflow can be complete, partial or absent. Velocity measurements are only possible for flows that achieve a certain minimum inundation depth of the instrument. Thus overflow was typically only measured for water levels greater than +1.0 mNHN. The results presented here are based on overtopping flow velocities for 1850 primary wave events. Values presented here are derived from curves fitted through the high-frequency measurements and thus do not account for instantaneous velocity spikes due to turbulence occurring at timescales shorter than 1 Hz.

To characterise loads originating from overflow phenomena the velocity parallel to the structure cross-section, which corresponds to the velocity along the x-axis  $V_x$ , is examined. The directionality of the load is given by the sign of  $\pm V_x$ ; positive values describe flow in downstream, seaward direction, and negative values denote flow in upstream direction (see Figure 13). Thus, for this study, positive (downstream) velocities are relevant for hydraulic loading of the lee side slope.

The statistical distribution of the flow velocities  $|V_x|$  over the groyne crest is shown in Figure 13. Tidal flow effects have not been removed here. Although the most common values are below 0.5 m/s, velocities in the downstream direction show a significantly larger proportion of higher values, indicating the higher loading caused by seaward travelling ships. Approx. 27 % of flows in downstream direction are over 1.0 m/s, whereas less than 13 % exceed this threshold in the opposite direction. The maximum flow velocities commonly exceed 2.0 m/s, in rare cases overflow velocities exceeding 3.0 m/s have been recorded.

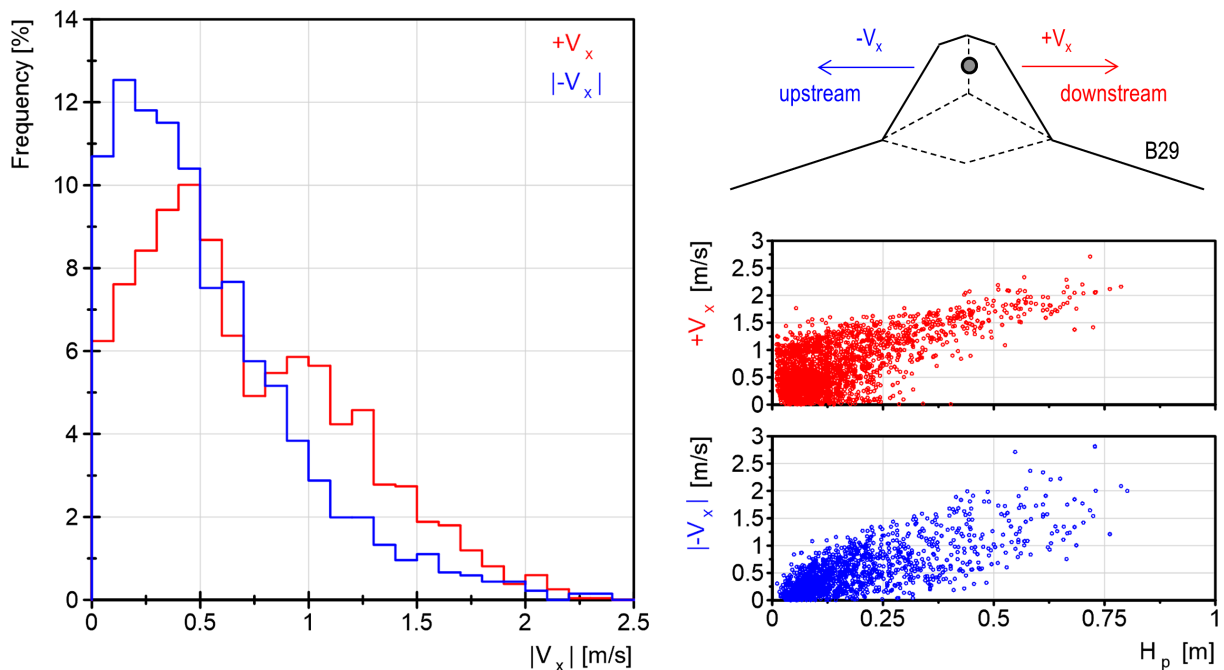


Figure 13: Frequency of occurrence of overtopping flow velocities at groyne B29 (left). Relationship between  $H_p$  and  $V_x$  (right).

The overflow process, as described by the event-associated parameter  $V_x$  is dependent on ship wave celerity, ambient (tidal) flow and modified by its interaction with and transformation over the structure. The relationship between the overflow velocity and the primary wave height at the groyne crest shows that flow velocities, in general, tend to scale with  $H_p$ .

## 4.2 Damage development

The damage to the armour layer is assessed by means of changes to the surface elevation between two surveys, as given by difference plots of the survey data. Figure 14 shows the deformation of the rock armour layer in the first groyne variants (B29v1, B31v1) and supporting photographic evidence taken on or close to the date of the survey. The difference plots represent the damage observed between the reference survey in July 2015 and another survey in April 2017, corresponding to a period of 645 days ( $\sim 1.75$  years). Over 6000 ship-induced long-period wave events were registered in this time period. For B29v1 some deformation of the crest and lee side slope area are observed; up to approx. 0.7 m of erosion are recorded here, with greater displacement of rock armour toward the groyne head. The wave-facing slope and the scour protection have remained stable. In contrast, groyne B31v1 displays much more severe deformation of the rock armour layer. The crest is

destroyed over nearly the entire length of the structure and erosion of 1.0–2.0 m, locally exceeding 2.0 m are observed. This has resulted in the exposure of historic groyne construction efforts, which form the core of the structure. The displaced rocks have been re-deposited, predominantly at the groyne foot on the lee side, as a result of the asymmetric loading from overflow events, leading to a flattened and widened appearance. The root area has remained remarkably stable.

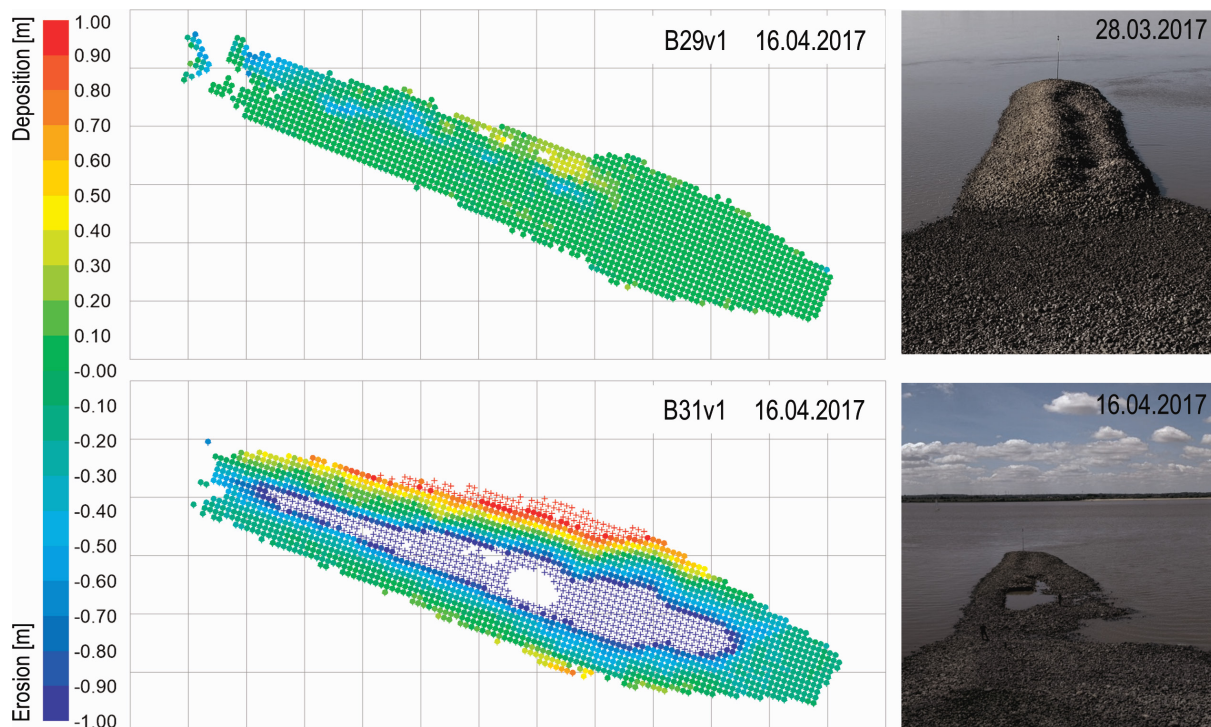


Figure 14: Damage development at B29v1 and B31v1 visualised as difference plots between 07/2015 and 04/2017. Crosses indicate exceedance of scale. Photographs of the groyne condition at or near time of survey.

The analysis of difference plots suggests that individual events, or the grouping of one or more relatively high-energy events can effect significant damages in the short period of time between consecutive low waters. One such example is illustrated in Figure 15 which shows the damage incurred at B31v1 between low water on the 4<sup>th</sup> and 5<sup>th</sup> of August 2015. A crest-parallel deformation of the lee side slope in the order of  $\pm 0.2$  m (average value for a 1 x 1 m raster cell) is observed, suggesting erosion on the order of approx. one layer of rock. Also shown are the wave events registered in this time. One extreme event with  $H_p = 2.3$  m, among other events of up to 1.0 m, was recorded. The largest event was associated with a vessel of 363 m length and 46 m breadth travelling seaward with 13.7 kn *STW* and 11.5 m draught at approximately mean water level. The vessel passed the groynes at a distance of 187 m.

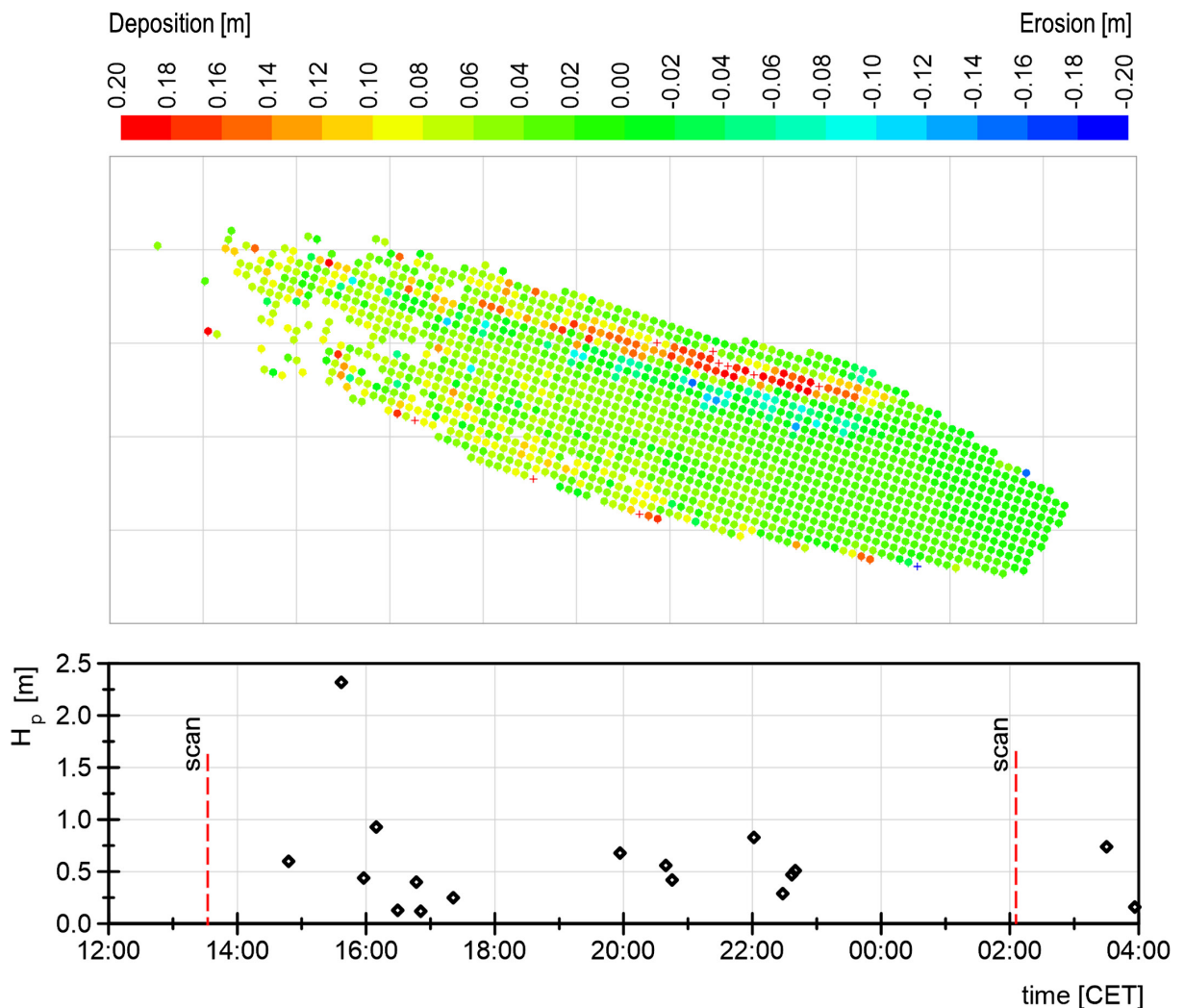


Figure 15: Damage development at B31v1 between two consecutive scans and measured wave heights at the groyne (pos. 5). Crosses indicate exceedance of scale.

Although B29v1 shows significantly enhanced rock armour stability compared to B31v1 despite the same rock grading, the observed damage after only 1.75 years did not satisfy the objectives of sufficiently increased armour layer stability. Subsequently, the groyne was rebuilt with a coarser grading of LMB<sub>5/40</sub> and a reference condition for variant B29v2 was scanned in November 2018. The changes to the rock armour over the time period of 442 days (~1.5 years) to the last scan in February 2019 shows only minor local deformation of typically less than 0.05 m on the wave-facing side and 0.1 m on the lee side (Figure 16). This can be attributed to an initial rearrangement and self-armouring of stones into a more stable position. The deformation pattern follows the previously described crest-parallel pattern, indicating the areas most affected by overflow events. The improved stability and condition of the rock armour layer was confirmed in recent manually conducted scan in December 2019 (Figure 16). It shows that after approximately two years, still very limited damage to the crest and lee side slope in the order of  $\pm 0.1$  m is recorded.

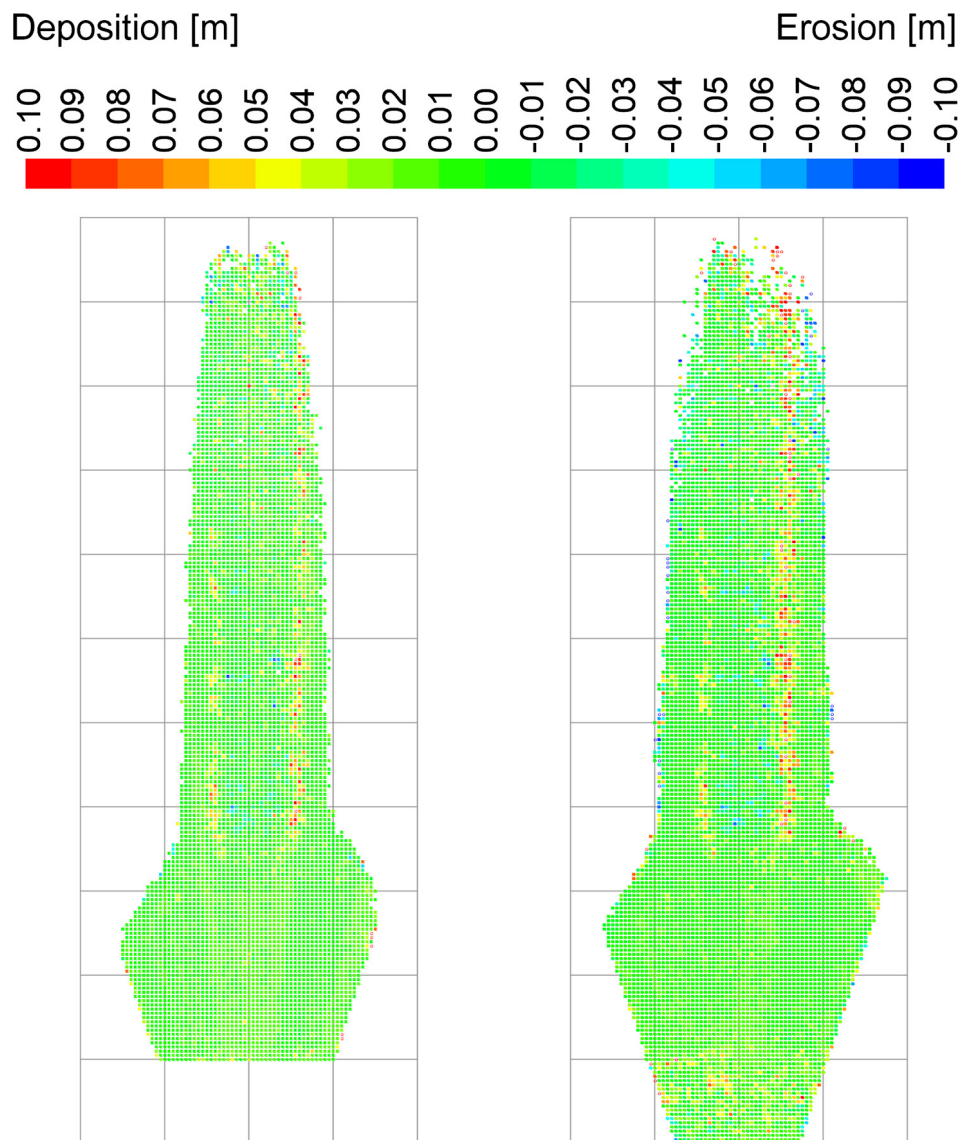


Figure 16: Damage development at B29v2 with larger rock size  $LMB_{5/40}$  visualised as difference plot between 11/2017 and 02/2019 (left) and 12/2019 (right).

## 5 Discussion of findings

### 5.1 Interpreting measured wave heights

The wave heights presented in section 4.1.1 were derived from statistics calculated over the entire monitoring period. While this is justifiable in order to present a simple first overview of loads, a more differentiated examination of the measurements is required to understand the important nuances of wave-structure interaction and groyne performance. As is the nature of prototype field studies, a large number of environmental variables remain uncontrolled, which poses some additional challenges in the correct interpretation of the measurements. Accounting for, as far as possible, the isolated and combined effects of these influencing factors is necessary for a true understanding of the measured wave loads. The major factors in this study are the deteriorating groyne condition, the vessel speed restriction and changes in groyne field morphology.

As shown in section 4.1, groyne damage typically manifests as a reduction in the crest level which in turn directly affects the wave-structure interaction, typically leading to lesser resistance to the wave. The measurements at B31, in particular, are strongly affected by this. As a result, wave heights at positions 4 and 5 tend to diminish with time. In contrast, the measured wave height at position 6 tends to increase with time, as the instrument is lowered with the deteriorating crest level. When examining the wave-structure interaction of a specific groyne design, only the measurements up to a certain damage condition will be representative of the performance. With respect to B31, the implication is that the actual hydraulic performance of the groyne design is somewhat misrepresented by a statistic over the entire period as presented here.

While the true impact of the speed restriction is yet to be examined, an analysis of the wave records at the groyne head has shown that the median wave height is reduced by approx. 1–2 cm, whereas more pronounced reductions are suggested at the other probe locations. This poses a challenge to the comparability of wave loads throughout the study period and implies that these two periods should be considered separately, when determining the stability of the rock armour to a certain load.

Further complication is given by the fact that groyne fields are subject to erosion and sedimentation through the monitoring period which in turn modulates wave transformation and energy dissipation in the nearshore area. Morphological changes were monitored in trimonthly profile surveys and analyses of this topographical data suggests that the beach levels display an average variability of approx.  $\pm 0.2$  to  $\pm 0.4$  m throughout the experiment.

Despite the mentioned caveats, the simple presentation of results chosen here allows a discussion of the general trends in wave-structure interaction and groyne performance. Further more detailed examination of the field data is currently being carried out to account for and untangle the contribution of the individual factors for the interpretation of wave heights. This will be required when conducting detailed investigations into the stability of the armour layer or secondary research questions such as e.g. the efficacy of the speed restriction in reducing wave heights on shoreline infrastructure and the understanding of groyne field morphological in the light of ship-borne loads, dredging activities and other environmental parameters.

## 5.2 Performance of optimised groyne designs

The key to increasing the stability of the armour layer that is subject to long-period ship waves is to reduce as far as possible the magnitude of flows over the groyne root and crest areas. In practice, this can be achieved by reducing wave focussing in the root area and increasing the dissipation of wave energy in the groyne field and at the structure. The latter can be achieved by reducing slope angles and increasing porosity of the structure slopes. While overflow cannot be practicably avoided in tidal waters, this study proves that the flow magnitudes can be reduced by means of design modifications.

While the wave height at the groyne head is largely independent of groyne design, the wave heights at locations around the groyne body reflect the wave's characteristic interaction with the structure (and nearshore) as it experiences dissipation, shoaling, reflection and refraction effects, thus allows the hydraulic performance of the groyne to be described and assessed with respect to reducing loads on the rock armour layer. One commonality of the

two designs is that the wave-facing side experience the largest wave heights as can be explained by the closer passing distances of seaward travelling ships. Wave heights increase toward the root area at both groynes due to wave shoaling, but also focussing and reflection effects. While this effect is quite pronounced at B31, it is much more subtle at B29 as the recess allows bypassing of wave energy through the root area. The smaller wave heights recorded at the crest of B29 in conjunction with the observation of much reduced damage suggests that fewer and less severe overflow events are experienced at the recessed groyne, despite the fact that no overflow was measured. At B31, arguably, the objective of improving the groyne root stability is achieved; however, this comes at the cost of an unfavourable increase in overflow loads over the groyne crest and body. At both groynes little to no damage is observed on the wave-facing side, leading to the conclusion that wave height alone is not the decisive factor in the structure deterioration and the load case  $R_c > 0$  is typically not problematic. It also implies that the overflow due to primary waves produced by ingoing vessels is also subcritical at this location.

In terms of forces acting on the crest and lee side slope, it has been shown that high velocities of up to 2.5 m/s are possible. When high-frequency turbulent velocity fluctuations ( $> 1\text{Hz}$ ) are considered the data shows that intermittently acting velocities can be significantly higher than the values quoted in section 4.1.2, with implications for additional lift and drag forces on the rocks in the armour layer. It is not surprising then to see the bulk of the damage occur at the crest and in particular at the lee side slope. It follows that the design conditions for the dimensioning of rock armour with respect to long-period waves is given by the load case  $R_c \lesssim 0$ , as hypothesized by BAW (2010) and Gier and Schüttrumpf (2012). Analysis of the relationship between the measured overflow velocities and corresponding wave heights at B29 have shown that  $V_x$  appears to scale with the wave height; thus an increase in wave energy at the crest will tend to increase the flow velocities and shear stresses on the crest and lee side slope. Further, the most damaging situation will arise when a large stern wave coincides with a large drawdown and a tidal water level which is conducive to maximising the length of exposed lee slope, assumed to typically occur around  $R_c \approx 0$ . With decreasing freeboard ( $R_c < 0$ ), the potential for higher flow volumes increases whereas the exposed length of slope is reduced, the exact configuration of these two parameters being specific to each ship passage. While flow velocities are an indication of destabilising forces, typically the overflow volume will be more relevant in determining rock armour stability. Ways of determining overflow volumes from this field data set with a view to estimating critical discharge values are currently being evaluated.

The intended function of the groynes, concentrating the flow in the main channel and supporting water levels during low water, is not forfeited by the recessed design. The groyne acts as a conventional groyne during low water as the recess is above the discharge-relevant wetted perimeter. The morphological developments in the groyne fields show that no erosion effects arise from the recessed root. Adverse array effects on morphodynamics arising from multiple recessed groynes seem unlikely, however should be considered in any scheme implementation. Negative impacts on the stability of the adjoining revetment was also not observed.

### 5.3 Increasing the stability of rock armour layers

A number of different approaches can be adopted to increase the stability of rocks in the armour layer. This includes e.g. the use of a larger rock size or higher density rock (in conventional or optimised design), geometry optimisation for improved wave-structure-interaction as attempted in this study or management options to reduce ship-borne wave heights.

In the case of structural damage, using a larger rock grading or higher density rock is always a potential remedy. The damage pattern suggests that an increase in rock grading on the crest and lee side slope only could also be a viable solution. To date there is no valid method to determine the adequate rock size for groyne overflow from long-period waves, thus the choice of rock grading has to be based on engineering expertise, knowledge of local conditions or, in the worst case, trial and error. The prototype observations have confirmed the dominance of overflow processes for the deterioration of the groyne rock armour. In this sense, there are parallels with phenomena in the field of hydraulic engineering such as weir flow and critical flow on riprap-armoured embankments and spillways with their respective empirical formulae (e.g. Isbash 1935, Abt et al. 2013). However, there are also important distinctions which are characteristic to long-period ship waves such as the influence of the dynamics and momentum of the wave on the destabilisation of rocks. Further it has to be considered whether spillway flow can develop in a meaningful way considering the wave dynamics and the exposure time of the lee side slope to the overflow (Gier and Schüttrumpf 2012). Work is currently ongoing to determine the suitability of these methods for rock sizing.

This study has shown that structural resilience can be increased by improving the wave-structure-interaction. The recess has shown to be effective in reducing hydraulic loads. Further optimisation should be explored, e.g. by assessing the performance of the recess as a singular measure, i.e. retaining the conventional groyne profile without changing side and head slope angles. A beneficial side effect of the recessed groyne can be in the promotion of aquatic habitats. Varying flow patterns in groyne fields with implications for their morphological and sedimentological make-up has been shown to increase the diversity of aquatic habitats in non-tidal rivers in Kleinwächter et al. 2017. Similar diversifying effects can be expected in estuaries.

Mitigating the wave loads at the source is also possible, but requires an understanding of how the nautical factors, in particular those that can be managed by vessel traffic regulations, influence the height of the near-shore wave at a specific site. Although the physics indicate the expected correlations between nautical parameters and incident primary wave heights, examination of the relationships in the field data set shows significant scatter, as would reasonably be expected. Nevertheless, certain parameter constellations can be identified which appear to favour the occurrence of large waves. At the study site for example the largest waves appear to be facilitated by conditions of highest vessel speed and channel blockage. Channel blockage is given by the blockage factor  $S = A_C / A_S$ , the ratio of the cross-sectional area of the waterway  $A_C$  and the ship's immersed midship-section  $A_S$ . It follows, that the blockage factor in a certain waterway cross-section is a function of ship breadth, draught and water level. To also account for the passing distance, the partial channel blockage factor  $S_P = A_{C,p} / A_{S,p}$  is introduced. Hereby only the part of the waterway cross-section and immersed midship-section comprising the area between vessel centreline

and the relevant shoreline is used as illustrated in Figure 17. The largest waves occur at high blockage, i.e.  $S_p$  ratios of approx. 5–10 (see Figure 18).

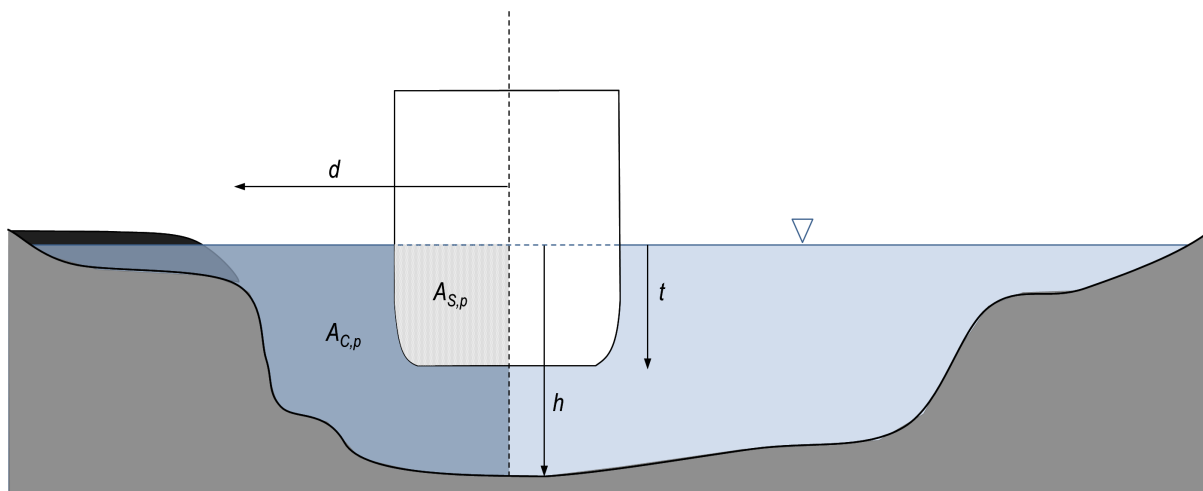


Figure 17: Definition of partial channel blockage factor  $S_p$  with immersed partial midship-section  $A_{S,p}$ , partial waterway cross-section  $A_{C,p}$ , passing distance  $d$ , water depth  $h$  and draught  $t$ .

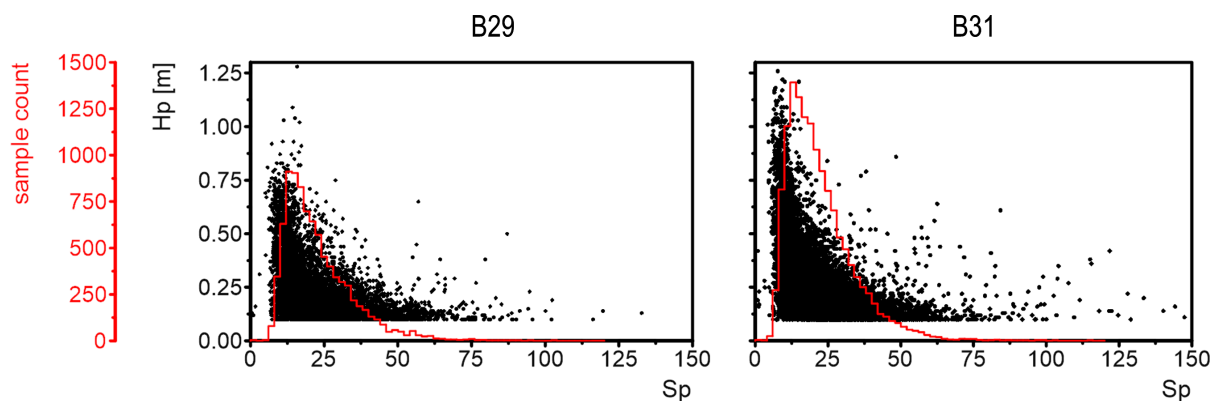


Figure 18: Influence of partial channel blockage factor  $S_p$  on primary ship wave height  $H_p$  at the heads of groynes B29 and B31. Sample count in red.

Figure 19 also shows the vessel speed through water in relation to the long-period wave heights. It can be observed that the maximum wave heights increase with speed until approx. 15 kn. Beyond that greater scatter and reduced sample size is observed. One factor contributing to the scatter is the fact that high-speed passages are often associated with smaller feeder ships, which despite the higher  $STW$  tend to produce smaller waves than ULCVs due to the lower partial channel blockage (high  $S_p$  value).

Quantifying the relative contribution of individual factors amongst other nautical and environmental parameters requires a more detailed examination. It is clear that while all these relationships have implications for the efficacy of wave height reduction, vessel speeds is the factor most readily accessible for regulation. Work is ongoing to determine in more detail the influence of a vessel speed on wave heights at the shore.

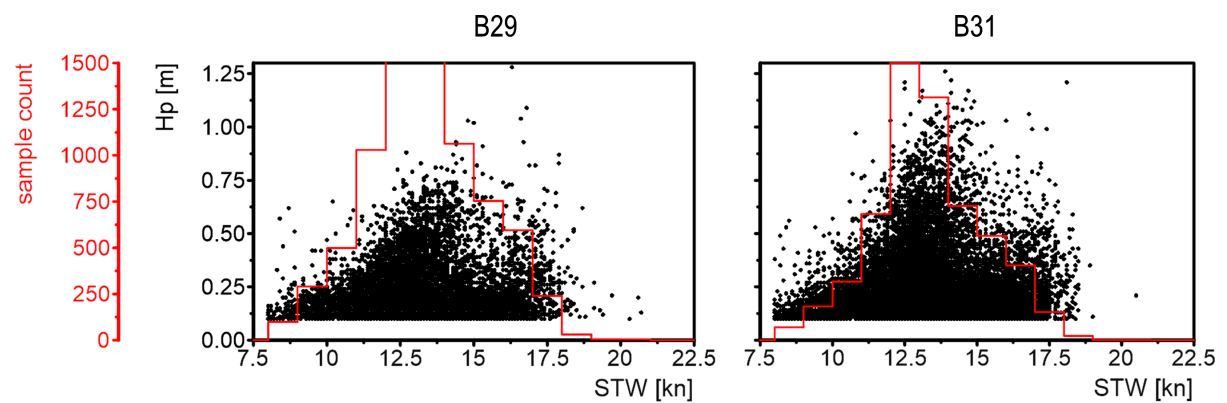


Figure 19: Influence of vessel STW on primary ship wave height  $H_p$  at the heads of groynes B29 and B31. Sample count in red.

## 6 Conclusions and further work

The conducted research programme has increased the understanding of the interaction between long-period ship waves and groynes. The measured hydraulic loads and damage development offer valuable insights into the mechanisms and processes leading to damage, but also leads for mitigation strategies.

Rock armour structures in German estuaries, designed decades ago in accordance with existing engineering guidance, are in some cases under-dimensioned to withstand the present-day ship-induced long-period waves, especially where waterway and nautical characteristics exacerbate the loading situation. While the highest wave impact is experienced on the wave-facing side, no damage is typically experienced here. The structural damage to groynes is related to high-velocity turbulent overflow phenomena to which the root, crest and lee side slope are particularly vulnerable. The most critical load case likely occurs when the ship wave with large drawdown and stern wave coincides with a relative water level that facilitates large volumes of flow over the groyne root and body. Modifications to structure geometry are shown to be effective in reducing loads by improving wave focussing and reflection performance. In particular, creating a recess in the groyne root offers these advantages as demonstrated in the measurably increased armour layer stability. The intended functionality of the groyne is not forfeited. Long term performance will be continually monitored, albeit in a much reduced scope, with wave height measurements at positions 1 and 5 of groyne B29 and visual assessments of structure condition.

To date, no validated engineering approach for the dimensioning of the rock armour layer in response to long-period ship waves is available. This dataset offers an opportunity to work towards a design methodology based on real prototype observations, as opposed to physical model tests. As such, further efforts are being directed towards evaluating and developing design methods. This includes exploring the applicability of design methods for weir flow and spillway erosion protection. The data will also be used in an attempt to develop a probabilistic design method.

While further optimisation of the groyne design is proposed, it is also important to consider the life cycle cost which considers construction as well as long-term maintenance frequency in comparison to conventional design with a larger rock size.

The data, although not collected specifically for this purpose, will also be used to shed light on questions of estuary management, e.g. examining the pattern and drivers of

morphological change in the groyne fields and a more in depth evaluation of the efficacy of the speed restriction in reducing wave heights at the shoreline.

## 7 References

Abt, S. R.; Thornton, C. I.; Scholl, B. A.; Bender, T. R.: Evaluation of overtopping riprap design relationships. In: *Journal of the American Water Resources Association*, 49 (4), 2013.

BAW: Bemessung der Strombauwerke in der Außenweser unter Berücksichtigung von Schiffswellenbelastungen (BAW-Gutachten, A39550210120), Bundesanstalt für Wasserbau, Hamburg, 2010.

BAW: Schiffserzeugte langperiodische Belastung zur Bemessung der Deckschichten von Strombauwerken an Seeschiffahrtsstraßen, AP1 – Schadensanalyse (BAW-Gutachten, A39550270141), Bundesanstalt für Wasserbau, Hamburg, 2012.

BAW: Schiffserzeugte langperiodische Belastung zur Bemessung der Deckschichten von Strombauwerken an Seeschiffahrtsstraßen, Arbeitspaket 4b, Kleinmaßstäbliche 3D-Untersuchungen zu alternativen Buhnsystemen (BAW-Gutachten, A39550270141), Bundesanstalt für Wasserbau, Hamburg, 2015.

BAW: FuE-Abschlussbericht, Schiffserzeugte langperiodische Belastung zur Bemessung der Deckschichten von Strombauwerken an Seeschiffahrtsstraßen, B3955020470141, Bundesanstalt für Wasserbau, 2018.

CIRIA, CUR and CETMEF: *The Rock Manual. The use of rock in hydraulic engineering*, 2nd edition. C683, CIRIA, London, 2007.

EAK: Empfehlungen für die Ausführung von Küstenschutzwerken durch den Ausschuss für Küstenschutzwerke der DGG e. V. und der HTG e. V. *Die Küste*, 65, 2002.

Gelinas, M. Bokuniewicz; H., Rapaglia, J.; Lwiza K. M. M.: Sediment resuspension by ship wakes in the Venice Lagoon. In: *Journal of Coastal Research*, 29, 8–17, 2013.

Gier, F.; Schüttrumpf, H.: Schiffserzeugte langperiodische Belastung zur Bemessung der Deckschichten von Strombauwerken and Seeschiffahrtsstraßen, Arbeitspaket 2: Wissensstandsanalyse der an der Wellen-Strombauwerk-Interaktion beteiligten Belastungsprozesse, Lehrstuhl und Institut für Wasserbau und Wasserwirtschaft, RWTH Aachen, 2012.

Göransson, G.; Larson, M.; Althage, J.: Ship-generated waves and induced turbidity in the Göta Älv River in Sweden. In: *Journal of Waterway, Port, Coastal and Ocean Engineering*, 140, 3, 2014.

Hansen, U.: *Wasserbausteine im Deckwerksbau, Bemessung und Konstruktion*, Westholsteinische Verlagsanstalt Boyens & Co, Heide, 1985.

Isbash, S.: *Construction of dams by dumping stones into flowing water*. War department, United States Engineer Office, Engineering Division, Eastport, Maine, 1935.

Kleinwächter, M.; Schröder, U.; Rödiger, S.; Hentschel, B.; Anlauf, A. (Hg.): *Alternative Bühnenformen in der Elbe – hydraulische und ökologische Wirkungen. Konzepte für die*

nachhaltige Entwicklung einer Flusslandschaft, Bd. 11. Schweizerbart Verlag, Stuttgart, 2017.

Niehüser, S.; Ulm, M.; Arns, A.; Jensen, J.; Kelln, V.; Uliczka, K.; Kondziella, B.: Interaction between ship-induced stress and associated characteristics of turbidity records. In: Uliczka, K.; Böttner, C.-U.; Kastens, M. et al. (Hg.): Proceedings of the 4th MASHCON 2016, Hamburg. International Conference on Ship Manoeuvring in Shallow and Confined Water with Special Focus on Ship Bottom Interaction, 2016.

Oetjen, J.; Lechthaler, S.; Schüttrumpf, H.: Schiffserzeugte langperiodische Belastung zur Bemessung der Deckschichten von Strombauwerken and Seeschiffahrtsstraßen, AP4-3 – Modellphase 3, Lehrstuhl und Institut für Wasserbau und Wasserwirtschaft, RWTH Aachen, 2017.

Ohle, N.; Zimmermann, C.: Untersuchungen zu den Ursachen von Deckwerksverwerfungen am Nordufer der Elbe. Mitteilungen des Franzius-Instituts für Wasserbau und Küsteningenieurwesen der Universität Hannover, 89, 155–198, 2003.

Oumeraci, H.; Kortenhaus, A.; Allsop, N. W. H.; de Groot, M. B.; Crouch, R. S.; Vrijling, J. K.: Probabilistic Design of Caisson Breakwaters and Sea Walls – Present Status and Perspectives. Proceedings of the 27th International Conference on Coastal Engineering, Sydney, Australia, 2000.

Oumeraci, H.; Brühl, M.: Schiffserzeugte langperiodische Belastung zur Bemessung der Deckschichten von Strombauwerken and Seeschiffahrtsstraßen, Arbeitspaket AP3: Bestimmung der bemessungsrelevanten Parameter schiffserzeugter Wellen in Seeschiffahrtsstraßen (Parametrisierung der Schiffswellen), Leichtweiß-Institut für Wasserbau, Technische Universität Braunschweig, 2013.

Oumeraci, H.; Brühl, M.; Neuert, N.: Schiffserzeugte langperiodische Belastung zur Bemessung der Deckschichten von Strombauwerken and Seeschiffahrtsstraßen – Arbeitspaket AP5: Entwicklung eines 3D-CFD/CSD-Modells und numerische Stabilitätsuntersuchungen (Numerische Simulation). Leichtweiß-Institut für Wasserbau, Technische Universität Braunschweig, 2014.

Parnell, K.; Soomere, T.; Zaggia, L.; Rodin, A.; Lorenzetti, G.; Rapaglia, J.; Scarpa, G.-M.: Ship-induced solitary Riemann waves of depression in Venice Lagoon. *Physics Letters A*, 379, 6, 555–559, 2015.

Rapaglia, J.; Zaggia, L.; Ricklefs, K.; Gelinis, M.; Bokuniewicz, H.: Characteristics of ships' depression waves and associated sediment resuspension in Venice Lagoon, Italy. In: *Journal of Marine Systems*, 85, 45–56, 2011.

Ravens, T. M.; Thomas, R. C.: Ship wave-induced sedimentation of a tidal creek in Galveston bay. In: *Journal of Waterway, Port, Coastal and Ocean Engineering*, 134, 21–29, 2008.

Scarpa, G.-M.; Zaggia, L.; Manfè, G.; Lorenzetti, G.; Parnell, K.; Soomere, T.; Rapaglia, J.; Molinaroli, E.: The effects of ship wakes in the Venice Lagoon and implications for the sustainability of shipping in coastal waters. *Scientific Reports* 9, Article number 19014, 2019.

Sehili, A.; Lang, G.; Lippert, C.: High-resolution subgrid models: background, grid generation and implementation. In: *Ocean Dynamics*, 64, 519–535, 2014.

Tschirschwitz, F.; Mechelke, K.; Jansch, H.; Uliczka, K.; Kersten, T.: Ein automatisches Monitoringsystem für Buhnen an der Elbe durch terrestrisches Laserscanning. In: ZFV – Zeitschrift für Geodäsie, Geoinformation und Landmanagement, 141, 297–305, doi: 10.12902/zfv-0132-2016, 2016.

Tschirschwitz, F.; Mechelke, K.; Kersten, T.: Automatisches geodätisches Monitoring von Strombauwerken an der Tideelbe bei Juellssand im Zeitraum Februar 2015 bis Januar 2017. HafenCity Universität Hamburg, Labor für Geomatik, 2017.

Ulm, M.; Niehüser, S.; Kondziella, B.; Arns, A.; Jensen, J.; Uliczka, K.: Field measurements in the Kiel Canal, Germany: Ship waves, drawdown and sediment transport. In: Journal of Waterway, Port, Coastal and Ocean Engineering, 146, 4, 04020020, 2020

Wöffler, T.; Oetjen, J.; Krebs, V.; Schüttrumpf, H.: Schiffserzeugte langperiodische Belastung zur Bemessung der Deckschichten von Strombauwerken and Seeschiffahrtsstraßen, AP4a – Vorversuche zur Modellphase 3, Lehrstuhl und Institut für Wasserbau und Wasserwirtschaft, RWTH Aachen, 2015.

WSA Bhv: Strombaulicher Bericht über den derzeitigen Stand der Bauwerksunterhaltung an den Buhnen und Leitwerken in der Außenweser, WSA Bremerhaven, 2009.

WSA Cux: Strombaulicher Bericht zur Bauwerksunterhaltung und zum Ufersicherungskonzept am Niedersächsischen Ufer, WSA Cuxhaven, 2012.

WSA HH: Buhnen Juellssand Dokumentation, WSA Hamburg, 2010.

Zaggia, L.; Lorenzetti, G.; Manfé, G.; Scarpa, G. M.; Molinaroli, E.; Parnell, K. E.; Rapaglia, J. P.; Gionta, M.; Soomere, T.: Fast shoreline erosion induced by ship wakes in a coastal lagoon: Field evidence and remote sensing analysis. PLoS One, 12, 10, e0187210, 2017.